Single-cell electro-mechanical cytometry

Junyu Chen, Daniel C. Spencer and Hywel Morgan*

School of Electronics and Computer Science, and Institute for Life Sciences University of Southampton, Southampton, SO17 1BJ, UK

Abstract

The complex structural and molecular features of a cell lead to a set of specific dielectric and mechanical properties which can serve as intrinsic phenotypic markers that enable different cell populations to be characterised and distinguished. We have developed a novel microfluidic technique that simultaneously measures both the electrical and mechanical properties of single cells at high speed. Cells flow along a microchannel and are deformed (elongated) to different degrees by the shear force created by a viscoelastic fluid and channel wall. The electrical impedance of each cell is measured along orthogonal axes to determine the shape change and thus the electrical deformability, along with cell dielectric properties. The system performance was evaluated by measuring the electro-mechanical properties of cells treated in different ways, including osmotic shock, glutaraldehyde cross-linking and cytoskeletal disruption with cytochalasin D and latrunculin B. This novel cytometer has a throughput of ~100 cells s⁻¹ is simple, and does not require sheath flow or rely on high speed optical imaging

Introduction

Label-free single cell analysis methods are of growing interest because they provide direct measurement of phenotype, particularly mechanical or electrical properties. The mechanical properties manifest through cell deformability are closely related to intracellular structure, particularly of the cytoskeleton and nucleus¹. Many different properties are linked to cell deformation, including cell cycle^{2,3}, cancer^{4,5,6} immune cell activation^{7,8} and stem cell differentiation^{6,9}. Single cell mechanical phenotyping can be performed direct from biopsy samples in order to determine inflammation and discriminate healthy from tumour tissue¹⁰.

Single-cell mechanical analysis is performed using several different techniques¹¹, including AFM^{12,13}, acoustic scattering¹⁴, optical stretching¹⁵, and micropipette aspiration¹⁶. However, these methods are not high throughput and can be technically demanding, and to address this microfluidic single cell cytometric methods have been developed¹. One technique is contact-based deformability cytometry (cDC), where cell stiffness is determined from the transit time as it squeezes through a narrow constriction. The transit time is measured using techniques such as optical imaging^{17,18,19} resonating cantilever methods (which can also determine cell buoyant mass)²⁰, or electrical resistance/impedance methods^{21,22,23,24}, including electrical node pore sensing²⁵. Constriction based methods have also been developed to characterise both the electrical and mechanical properties of single cells²⁶. However, contact based methods are generally low throughput, influenced by clogging of the channel and measure a narrow range of cell sizes. Furthermore, cell transit time is influenced not only by deformability but also by cell volume and membrane-wall friction and interactions.

To address these limitations non-contact analysis methods have been where a hydrodynamic flow induces a shape change in the cell, eliminating interaction between the cell and the channel wall. High speed cameras and image processing measure cell shape from which cell deformability is inferred. Shear flow deformability cytometry (sDC) uses strong velocity

gradients to generate shear stress in a microchannel slightly larger than the cell to deform the cell into a bullet shape^{27,28}. Shear forces dominate, and this technique is mostly sensitive to changes in the cytoskeleton but not the nuclear structure.

Extensional flow deformability cytometry (xDC) uses fluid-induced stress to deform cells at a stagnation point, normally with a cross shaped microfluidic channel^{5,6,29}. Inertial forces induce changes in a few micro-seconds meaning that analysis rates exceed 1,000 cells per second (high *Re*). The dominant compressional force from the fluid inertia deforms the cells. Guillou et al³⁰ used an extensional flow device but at much lower Re numbers where shear forces dominate and observed changes due to actin destabilisation. Armistead et al³¹ described a device that covers both flow regimes from high to low strain in both shear and inertia dominant regimes and showed that different regimes probe different aspects of the cell structure, demonstrating that the shear-dominant, low-strain regime is most sensitive to cytoskeletal changes. The three different techniques were recently compared³², confirming that the higher strain rate of xDC makes measurement of cytoskeletal changes (actin destabilisation) challenging, possibly due to cytoskeletal fluidization³¹.

Analogous to the field of cell mechanics, probing cell phenotypic electrical properties has been of interest for many years. Traditionally cells were analysed in suspension, but microfluidic technologies enable high speed single cells, allow heterogeneity in populations to be identified. Cell electrical properties reflect fundamental cellular physiology, for example cell cycle³³, activation/function³⁴, cytoskeleton³⁵; and single cell impedance analysis has been used for tumour cell stratification/separation^{36,37}, leukocyte analysis³⁸ and to identify parasite invasion³⁹. Single cell impedance analysis is usually performed using microfluidic devices with micro-electrodes that measure the impedance of a microchannel as cells transit between successive pairs of electrodes^{40,41}. Traditionally measurements are made at two AC frequencies, typically a lower frequency (high kHz) to measure cell volume and a second higher frequency to measure cell membrane properties. The ratio of these two impedances is termed the electrical opacity⁴¹ and indirectly characterises the cell membrane. Single cell multifrequency measurements have also been demonstrated providing a complete electrical phenotype by fitting data to a lumped-parameter model⁴².

Given the growing interest in label free techniques, and their translational potential for diagnosing disease, techniques that simultaneously measure both the mechanical and electrical properties of cells may provide important insights into cell behaviour and disease pathology. Recently a non-contact impedance-based deformability cytometer was described⁴³. This system measures cell deformability using electrical rather than optical methods and measures both the electrical and mechanical properties of single cells at moderate throughput (10-20 cells per second). Viscoelastic-inertial sheath flow is used to focus cells into a narrow stream that flows through a cross-junction where cells are deformed due to pinching from sheath fluids. In this system shear force dominates over the compressive force. The change in cell shape was determined by comparing the impedance signal before and after a cell passes along the crossshaped microchannel. Size, deformability and electrical opacity of neutrophils was measured, demonstrating changes upon activation. Reale et al⁴⁴ used extensional flow created with a hyperbolic channel to induce cell deformation. Planar microelectrodes at a cross junction measure the orthogonal and lateral impedance to determine cell shape after deformation. Differences between normal RBCs and stiffer spherical RBCs (treated with SDS and Glutaraldehyde) were identified. Owing to variations in the electrical impedance signal with position in the channel, off-centre particles were discarded (based on velocity), corresponding to around 50% of total events.

In this paper we describe a high throughput single cell shear flow deformability cytometer (sDC) that simultaneously measures the mechanical and electrical properties of single cells at high throughput (>100s⁻¹). The method is simple and does not require a separate sheath flow or high-speed cameras with associated data processing overheads. Cells suspended in a viscoelastic buffer and are pumped through a narrow channel, producing a shear force to induce cell deformation whilst also focusing cells into the channel centre⁴⁶. Cell deformability and electrical properties are measured using integrated planar microelectrodes, at two discrete frequencies giving cell volume, shape and cell electrical properties. As a cell flows through a channel the electrical impedance is measured along two orthogonal axes to determine any change in the cell as it deforms (from sphere to ellipse) along with the electrical volume and opacity.

We demonstrate the utility of this technique by measuring the combined mechanical and electrical properties of HL60 cells under several different experimental conditions, including osmotic stress, Glutaraldehyde (GA) cross-linking, and cytoskeleton disruption. This new electro-mechanical phenotyping is simple and inexpensive. The system is high throughput, simple and does not require complex fluidics or sheath flow focusing and provides equivalent data to other optical deformability cytometry methods.

Principle of operation

The working principle of the system is shown in Figure 1(a). Cells are suspended in a viscoelastic fluid (0.5% w/v methylcellulose in DPBS) and pumped through a micro-channel ($40 \mu m$ wide, $28 \mu m$ high) at a flow rate around $10\mu L/min$. The viscoelastic fluid exerts a shear stress on cells as they enter the channel, leading to high deformation at low flow rates (Figure 1b) and (Supplementary Figure 1). It also focuses the cells into the centre of the channel, minimising the positional dependence of the impedance signals, eliminating particle-particle and particle-channel contact, and improving the stability of the cells in the flow. The change in cell shape is determined from the impedance signal recorded from the two sets of electrodes, as shown in the figure. One set generates an electric field orthogonal to the flow while the second set creates a field along the flow direction as shown by the vertical and horizontal electric field lines in Figure 1(a). Cells first enter the vertical field region (electrodes I_1 and I_2) where the cell volume is determined. The second set of electrodes generates a field along the flow direction (I_A , I_B and I_C , I_D) measuring the particle cross section along the flow direction from which the deformation of the cell is determined.

At low AC frequencies (<500kHz in saline) cells behave as electrical insulators so that the impedance signal is proportional to the electrical volume. An absolute volume measurement is obtained by scaling the impedance signals using solid polystyrene reference particles of known volume, mechanical and electrical properties⁴². Cell deformability is defined as the ratio of the low frequency vertical to lateral impedance ($\mathbf{Z}_1/\mathbf{Z}_2$) (Figure 1(a)). An example scatter plot of electrical deformability vs diameter for HL60 cells is shown in Figure 1(c). The electrical deformability of the undeformed calibration beads is set to 1.0; softer cells have values greater than 1.0.

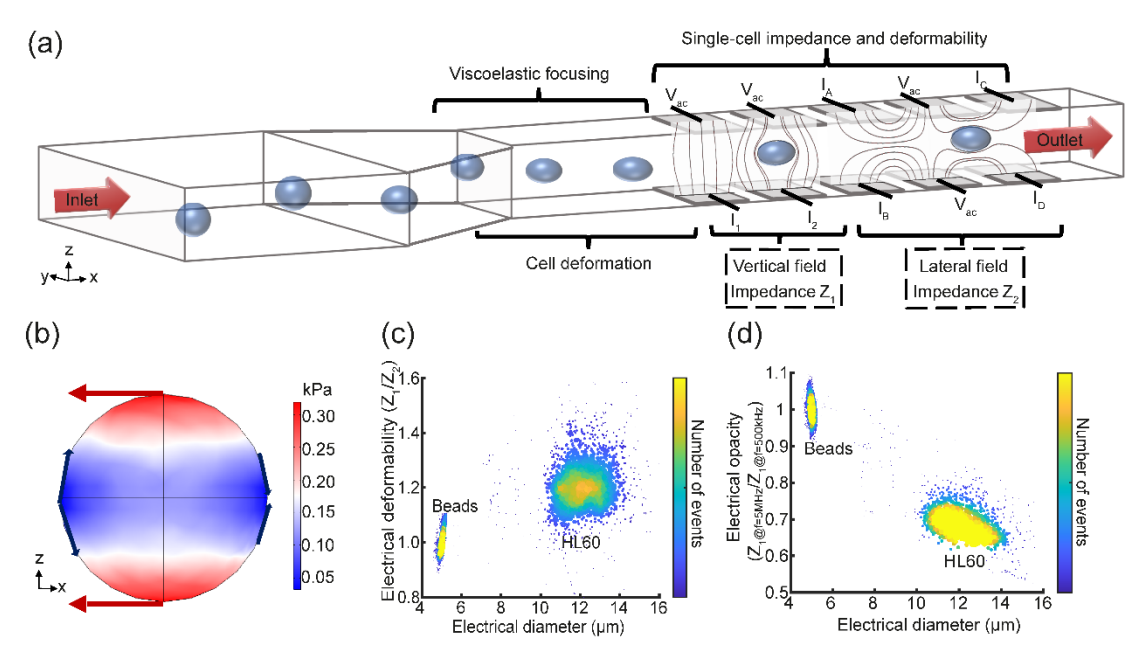


Figure 1(a) Principle of the electro-mechanical cytometer. Cells suspended in a viscoelastic buffer flow along a microfluidic channel within which there are two sets of microelectrodes. One set measures the cell volume (Z_1) whilst the second set measures cell deformation along the direction of flow (Z_2) . Cells are focused into the centre of the channel by the viscoelastic suspending fluid that is used to create the shear stress. (b) shows the shear stress on an undeformed sphere in a viscoelastic fluid $(0.5\% \text{ v/v} \text{ methyl cellulose}, 0.015 \text{ Pa·s}, \text{ density } 1005 \text{ kg/m}^3$, flow rate $10\mu\text{l/min}$, particle radius $6\mu\text{m}$), see ESI for further details. Arrows indicate direction of the local force. Density plots of electrical deformability (c) and electrical opacity (d) as a function of electrical diameter for HL60 cells (n=2,000) at a flow rate of $10\mu\text{l/min}$. $5\mu\text{m}$ rigid beads included as reference particles in both cases.

The impedance at higher frequencies (5MHz) provides information on the electrical properties of the membrane and cytoplasm. The ratio of this impedance to the low frequency is termed the electrical opacity and normalises for cell volume. Figure 1(d) shows a scatter plot of electrical opacity vs electrical diameter for the HL60 cells. The data is scaled to the opacity of homogenous solid dielectric beads (equal to 1.0 by definition)⁴². Biological cells with membranes have values lower than 1.0, and changes in opacity correlate with membrane capacitance and cytoplasmic properties.

Simulation

In order to understand the relationship between electrical impedance and cell deformation, a series of finite element simulations of the system were performed. The numerically calculated electric field for the electrodes is shown in Figure 2(a) along with the resulting time-dependent impedance signals, Figure 2(b). The figure shows that in the first set of electrodes (Z_1) the electric field is orthogonal to the flow and the impedance of an ellipsoid is slightly larger than the undeformed sphere. Z_2 measure the cross-section of the particle as it flows along the channel. For an ellipsoid, less current is blocked compared to a sphere resulting in a reduction in Z_2 . The impedance of an elongated object is therefore different from that of an undeformed object. Finally, the electrical deformability is determined from the ratio of the two impedances, Z_1/Z_2 .

The impedance of a particle depends on its vertical position in the channel⁴⁶ and several different approaches have been adopted to correct/compensate for this^{47,48,49}. This error was minimised through the use of an optimised electrode arrangement (see Supplementary Figure 2(a)) which together with the focusing effect of the viscoelastic medium (Supplementary Figure 3), ensures that the impedance from the first set of electrodes (Z_1) provides a good estimate of cell volume. The lateral impedance (Z_2) is more sensitive to both position and cell deformation (see Supplementary Figure 2(b) and (c)), but the viscoelastic focusing again ensures that most particles are confined to the central region of the channel. The vertical impedance Z_1 is also used to measure the electrical properties of the cells because these electrodes minimise the positional dependence of the signal.

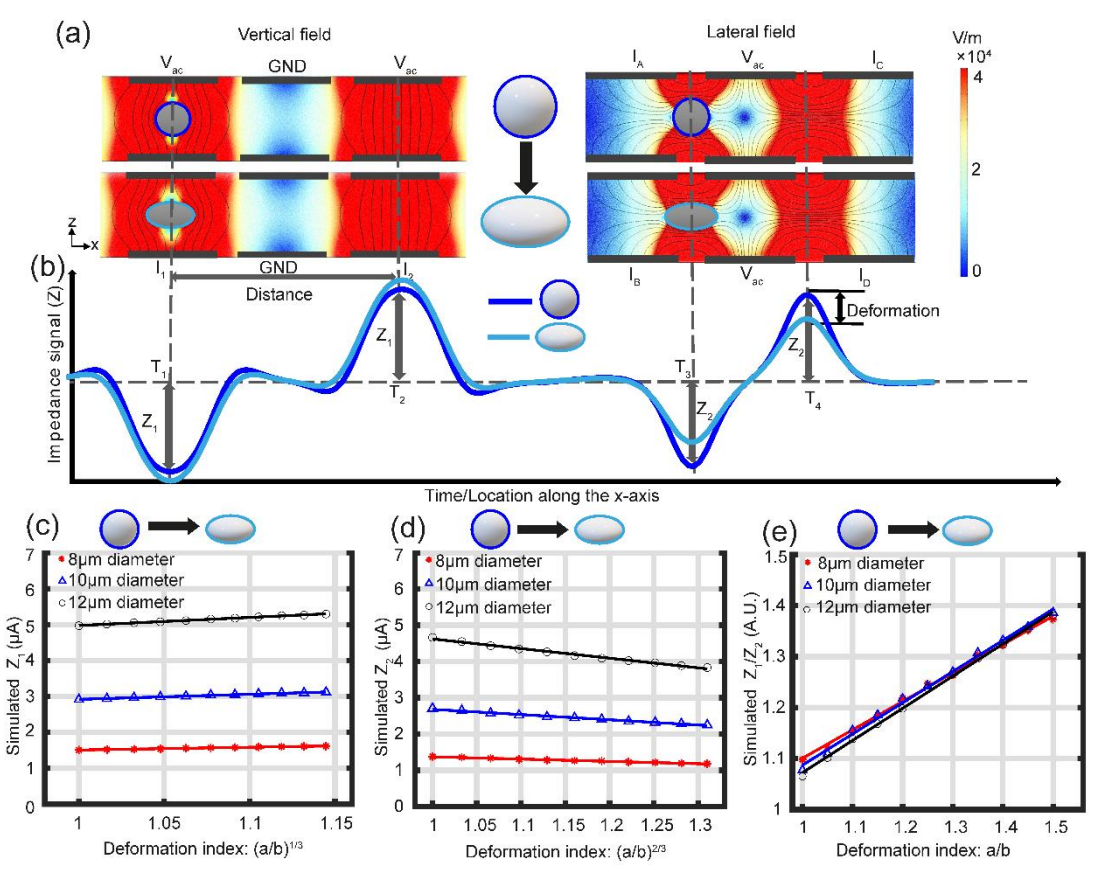


Figure 2 (a) Side view (z-x) of the vertical and lateral electric field for an applied voltage of $\pm 1V$. with a solid dielectric sphere and ellipsoid. Colour scale is the magnitude of the electric field (V/m). (b) The two sets of electrodes create an impedance signal consisting of two sets of antisymmetric bimodal Gaussians. (c) Sensitivity plots for vertical impedance Z_1 and (d) lateral impedance Z_2 as a function of the deformation index (major/minor axis) for three different sizes of particles. (e) Electrical deformability (Z_1/Z_2) as a function of the deformation index for three different sizes of particles. Particles were modelled as homogenous solid dielectric objects with specific conductivity and permittivity (ε_p =2.5 ε_0 and σ_p =2.7×10⁻³ S/m) and a frequency of 500kHz. Simulated channel dimensions are 200 μ m long, 28 μ m high and 40 μ m wide.

In order to quantify the expected change in impedance as particles deform, the current in the channel was numerically calculated for a series of solid ellipsoids with different major/minor axes. In each case the particle volume was kept constant. Defining major axis a and minor axes b = c, the ratio between a and b (= c) was varied from 1.0 (sphere) to 1.5 (ellipse) and the current calculated. This allowed the deformation index, defined as the ratio of major axis to minor axis (a/b) to be calculated.

For a fixed volume object the cross-sectional area of the vertical projection (A_v) as measured by Z_l is given by equation (1), whilst the cross-sectional area of the horizontal projection (A_h) is given by equation (2).

$$A_{v} = 2\pi \left(\sqrt[3]{\frac{3 \text{ Volume}}{4\pi}}\right)^{2} \sqrt[3]{\frac{a}{b}}$$

$$A_{h} = 2\pi \left(\sqrt[3]{\frac{3 \text{ Volume } b}{4\pi \ a}}\right)^{2}$$
(2)

$$A_{h} = 2\pi \left(\sqrt[3]{\frac{3 \text{ Volume } b}{4\pi \ a}} \right)^{2} \tag{2}$$

Figure 2(c) shows the vertical impedance Z_1 as a function of the cube root of the deformation index (a/b) for different particle diameters (equation (1)), demonstrating that the overall change is small, particularly for smaller particles. This trend can be compared with Figure 2(d) which shows how Z_2 varies with $(a/b)^{(2/3)}$, i.e. the horizontally projected area. Importantly the deformability determined from (Z₁/Z₂) is almost independent of particle size and is linearly proportional to particle aspect ratio (a/b), see Figure 2(e).

Experimental

Osmotic shock.

Mammalian cells exposed to hyperosmotic solutions (higher than 300mOsm) rapidly shrink and become much stiffer as the volume of the cytoplasm is reduced, leaving the majority of the internal volume occupied by the cell nucleus⁵⁰, as shown in Figure 3a. intracellular molecular crowding leads to an increase in cell stiffness and an increase in membrane folds which would manifest as an increase in the cell membrane capacitance. Therefore, a series of osmotic shock experiments were performed on HL60 cells using buffers of varying osmotic strength but with constant electrical conductivity. Prior to measurement, each group of cells was exposed to a different osmolarity-adjusted MC buffer for 10 minutes.

Figure 3 shows representative scatter plots of electrical deformability at 300mOsm (b) and 700mOsm (c) at a flow rate of 10µl/min. Contour plots (50% density) of deformability vs electrical diameter for different osmolarities is shown in Figure 3(d) demonstrating that both the electrical diameter and deformability reduce with increasing osmolarity. Figure 3(e) shows contour plots of electrical opacity vs. diameter for different osmolarity showing a decreasing trend in opacity with increasing osmolarity. This is consistent with the expected increase in membrane surface folds which in turn leads to an increase in cell membrane capacitance (i.e. the opacity at 5MHz decreases). Figure 3(f) summarises data for electrical diameter as a function of osmolarity at a flow rate of $10\mu l/min$ (n = 3), where the diameter decreases with osmotic pressure, a trend that is independent of the flow rate (Supplementary Table 1).

Figure 3(g) shows how electrical deformability decreases with osmolarity at different flow rates (n=3), demonstrating that the relative change increases with the flow rate (Supplementary Table 1) as the shear stress increases increasing the deformation of cells. Finally Figure 3(h) summarises the electrical opacity changes with osmolarity (at 10µl/min) demonstrating an increase in the membrane capacitance as the cells shrink. Different flow rates had little effect on the relative change in opacity. Both the deformability and size of HL60 cells decreased with increasing osmolarity consistent with previous reports³².

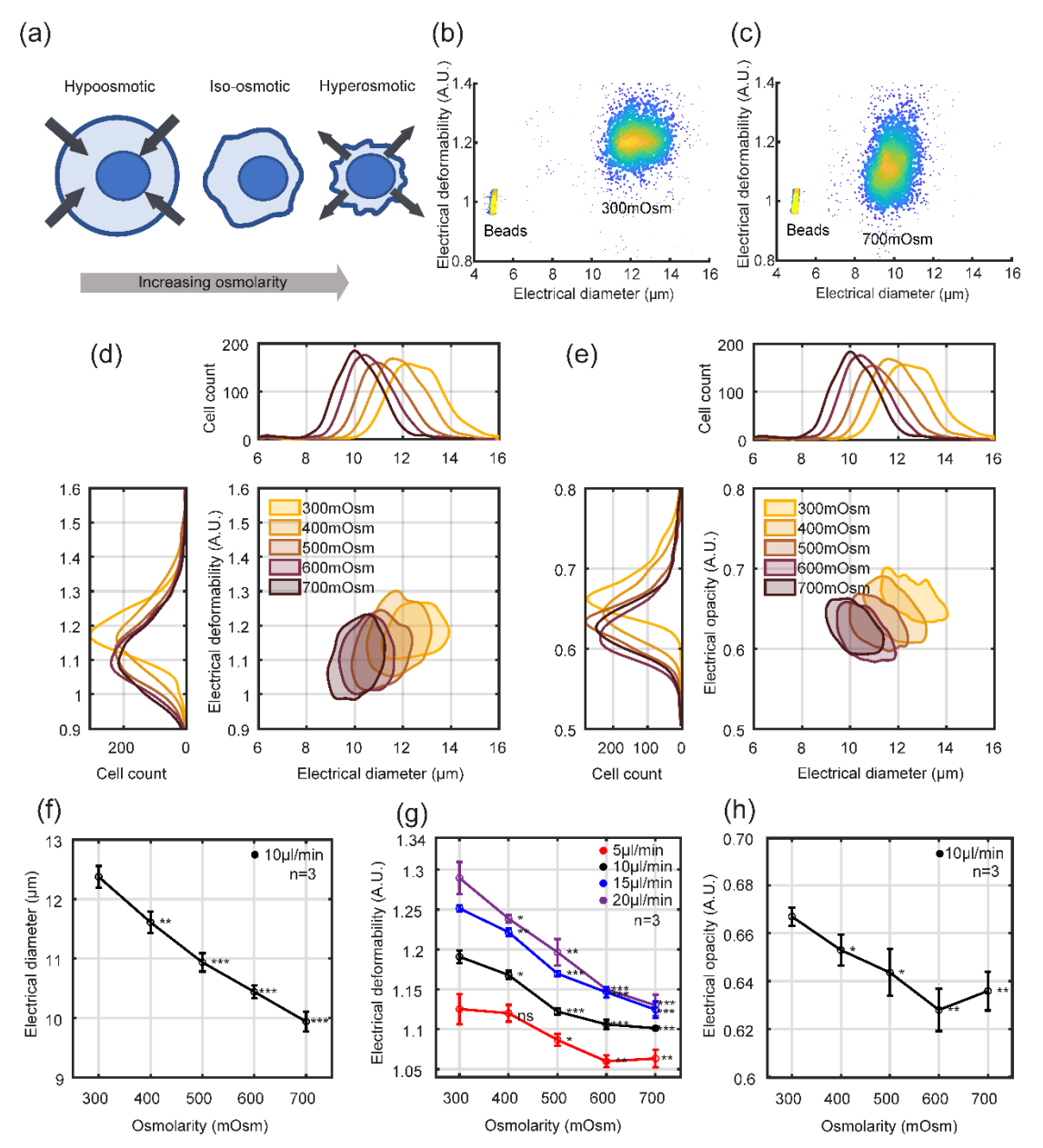


Figure 3(a) Increasing the osmotic pressure causes cells to shrink leading to an increase in membrane folds. (b) and (c) example density scatter plots of electrical deformability vs electrical diameter for 300mOsm and 700mOsm at a flow rate of 10μ l/min. (d) Contour plots (50% density) of electrical deformability vs electrical diameter for different osmolarities (flow rate 10μ l/min). (e) electrical opacity vs. electrical diameter for different osmolarities (flow rate 10μ l/min). Data is representative of one experiment. (f) Mean electrical diameter as a function of osmolarity (n=3). (g) Mean electrical deformability as a function of osmolarity for different flow rates (n=3). (h) Electrical opacity vs osmolarity at a flow rate of 10μ l/min, (n=3). P-values (student's t-test) are relative to cells measured at isotonic osmolarity (300mOsm). *** p<0.001, ** p<0.05, and ns significant. Number of cells in each group is approximately 2,000.

Sukhorukov et al⁵¹ demonstrated that the membrane surface area reduces as cells expand in hypoosmotic solutions, with a reduction in cell membrane capacitance before reaching a limiting value. As the cells swell in hypotonic solution, microvilli disappear to compensate for increasing membrane area. By contrast exposure to hypertonic solutions leads to shrinkage of

cells and collapse of the apical membrane onto the cortex⁵², so that the cells become much stiffer with an increase in cell membrane capacitance, as observed experimentally.

Cross-linking

It is known that cells become much stiffer after exposure to protein cross-linking using agents such as glutaraldehyde (GA) where deformability gradually decreases with increasing concentration^{53,54}. To study the dose-response of GA, HL60 cells were treated with different concentrations and the stiffness compared with unfixed control cells. Cross-linking with GA significantly altered both cell deformability and cell opacity. Figures 4(a), (b) and (c) show example scatter plots of electrical deformability vs electrical diameter at different concentrations of GA. At the highest concentration (0.1%v/v), the electrical deformability is around 1.0, similar to the control beads. Cell diameter was not influenced by GA treatment. Figure 4(d) shows contour plots (50% density) of electrical deformability vs diameter for different GA concentrations whilst Figure 4(e) shows a similar plot for the electrical opacity. Dose-response curves are shown in (f)) (g) and (h). No change was observed in cell size but significant differences were observed in cell deformability even at small concentrations of GA. Fitting this data to a four-parameter Hill equation, gave a half maximum concentration, $EC_{50} =$ 0.0014% v/v GA, consistent with deformability measurement made in spiral microchannels⁵³. Increasing the flow rate to 10ul/min, had a minimal influence on the electrical deformation, which remained similar to that at 5µl/min (Supplementary Figure 4a), with a similar EC₅₀ value (Supplementary Figure 4b).

Figure 4(h) summarises the mean electrical opacity vs GA (n = 4), where only the two highest concentrations (0.01% and 0.1% v/v GA) lead to significantly changes in cell electrical opacity. It has been shown that treatment of red blood cells with glutaraldehyde leads to cross linking of the protein networks that form the cell membrane and the cytoskeleton leading to an increase in opacity⁵⁵. This increased opacity was linked to decreased cytoplasm conductivity and decreased membrane capacitance, both resulting from protein cross-linking. Gagnon et al⁵⁶ showed that GA cross linking reduces membrane permittivity (from 10.5 to 3.8) for RBCs. Pribush et al⁵⁷ also showed that GA reduces the capacitance of RBC membranes.

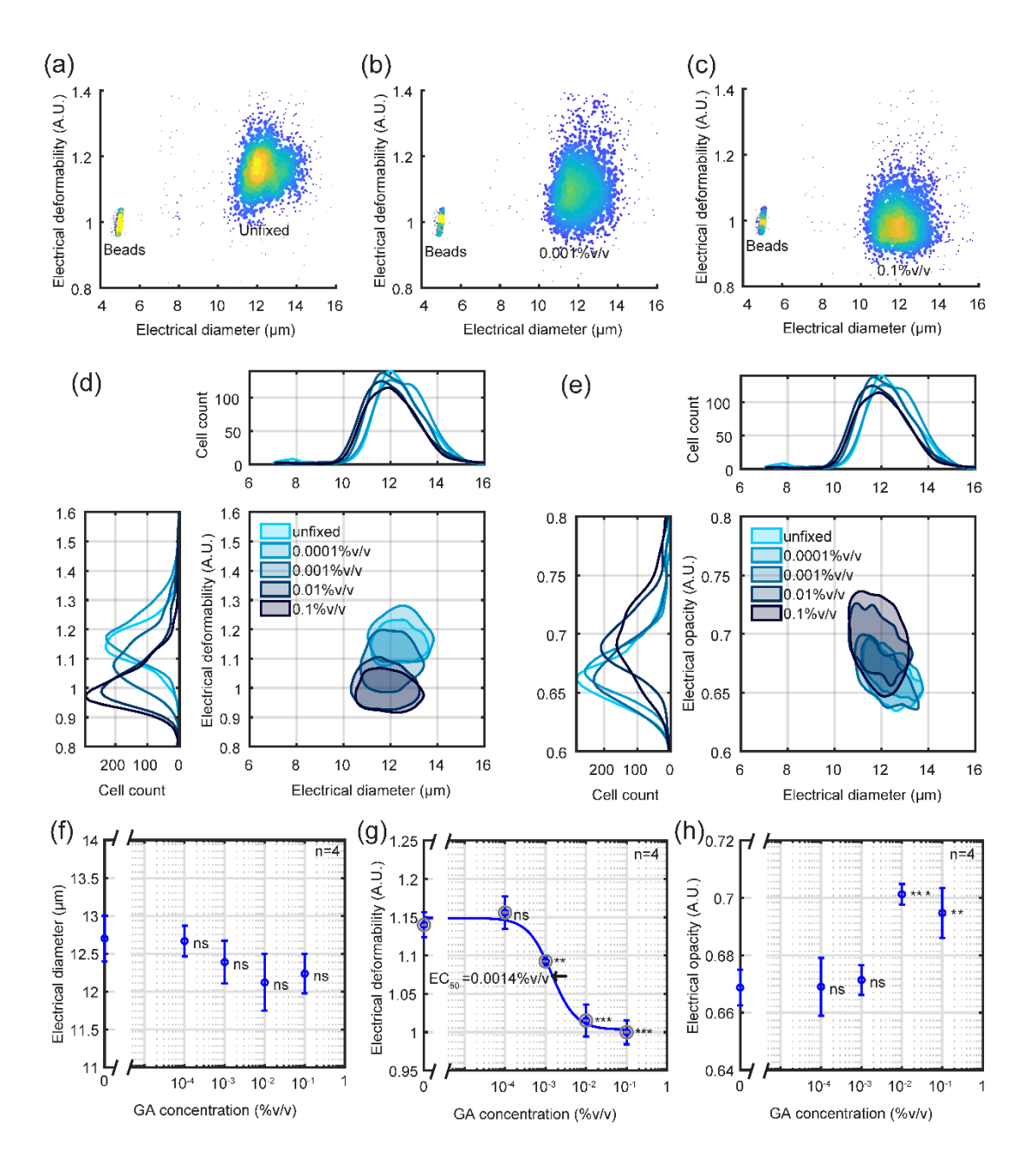


Figure 4. Example density plots of electrical deformability as a function of the electrical diameter for (a) unfixed, (b) 0.001% v/v and (c) 0.1% v/v GA fixed HL60 cells at a flow rate of 5μ l/min. Contour plots (50% density) of electrical deformability (d) and electrical opacity (e) vs electrical diameter. Dose-response data for electrical diameter (f), electrical deformability (g) and electrical opacity (h) at 5μ l/min. Error bars are standard errors of the mean for n=4. P-values (Student's t-test) are relative to unfixed cells (0%v/v). EC50 for electrical deformability = 0.0014% v/v. The number of cells in each group was approximately 2.000.

Cytoskeleton disruption.

The mechanical properties of the cytoskeleton of cells were altered by treatment with Cytochalasin D (CytoD) or Latrunculin B (LatB). CytoD inhibits actin filament elongation by binding to the barbed ends of the filaments preventing polymerisation, resulting in loss of cytoskeletal structure and decreased stiffness. LatB modulates cell stiffness by binding actin monomers, preventing them from polymerising the actin filaments. Example scatter plots

illustrating the effect of these compounds are shown in Figures 5 (a), (b) and (c) for control, 1μM CytoD and 0.25μM LatB demonstrating that exposure leads to a decrease in cell stiffness, consistent with observations from other groups^{32,43,58}. Contour plots of electrical deformability vs electrical diameter for different CytoD concentrations (at 5µl/min) are shown in Figure 5(d), (Supplementary Figure 5(a) for 10 µl/min). Cell diameter was not significantly affected by either Cyto D (Figure 5(f)), or Lat B consistent with other reports³² although Guzniczak⁵³ noted a small (10%) reduction in cell size measured by flow cytometry (FSC) for Cyto D as low as Dose-response curves were extracted from measurements of CytoD cells at different concentrations, yielding half-maximal concentrations of 17 nM (@ (5µl/min), Figure 5(g) or 11nM (@ 10µl/min) in good agreement with the previously reported values of 13.5nM⁵³. Figure 5(e) shows that electrical opacity is unaltered by exposure to CytoD, implying that destabilisation of the cytoskeleton has no statistically observable effect on the membrane or cytoplasmic properties as determined from the electrical opacity. This contrast with the results of Jaffe and Voldman³⁵ who measured the electrical properties of 262 cells exposed to Cyto D using a dielectrophoresis spring system. They observed differences between control and treated cells although no absolute values of the electrical properties were reported. These data were obtained using multiple frequencies up to 25MHz and furthermore, their system does not expose cells to shear stress making direct comparison difficult.

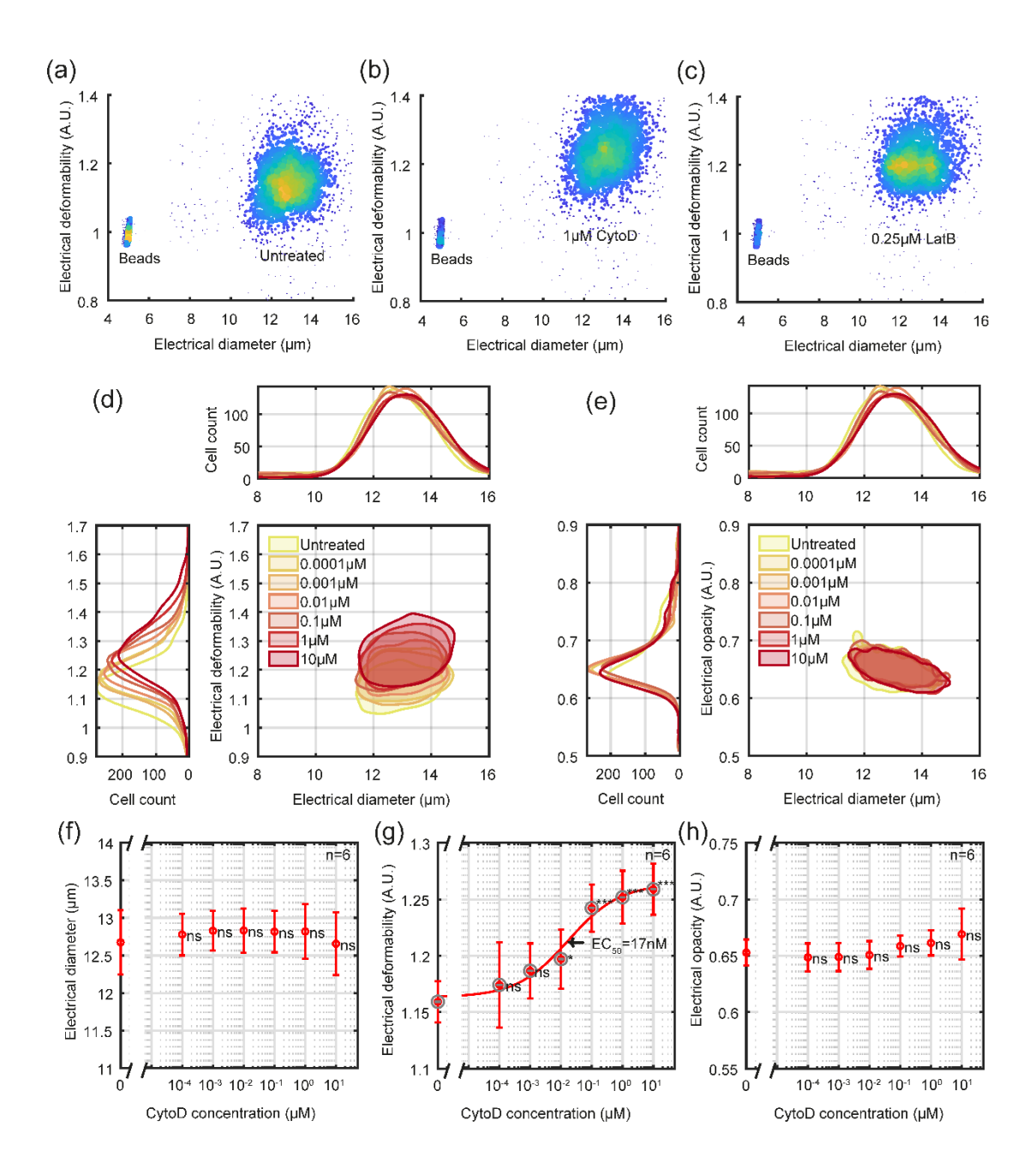


Figure 5 Density plots of electrical deformability vs electrical diameter for (a) untreated, (b) 1μ M CytoD and (c) 0.25μ M LatB treated cells. Contour plots (50% density) of (d) electrical deformability (d) and electrical opacity vs electrical diameter (e) for CytoD treated cells. Dose-response graph for electrical diameter (f), electrical deformability (g) and opacity (h). CytoD deformability EC50 for = 17nM. Error bars are standard errors of the mean value of n=6. P-values (Student's t-test) are relative to untreated cells. All data collected at a flow rate of 5μ l/min.

Conclusion

We have developed a shear flow deformability cytometer (sDC) that can measure the electromechanical properties of single cells at high throughput. The cytometer was used to characterise changes in cells exposed to different chemical/physical stress demonstrating concordance with other optical techniques. This new cytometer has several advantages. The technology is relatively simple and does not require high-speed cameras, and the associated image processing. Detection of single cell events using impedance could be used to trigger

image capture with a low-cost CMOS camera. The system could be useful for drug screening or even as a test to diagnose disease that affect the electro-mechanical properties of cells. Furthermore, high-speed signal processing of the electrical signals could lead to the development of a high-speed cell sorting systems based furthering the understanding of cell heterogeneity and the links between electro-mechanical phenotype and disease at the single cell level.

Methods

Impedance analysis

The electrical properties of single cells were measured using two superimposed frequencies 500kHz (lf) and 5MHz (hf). The current change from the electrodes is converted to voltage with a custom trans-impedance amplifier. A lock-in amplifier ((HF2LI, Zurich Instruments) demodulates the signals separating the real and imaginary parts. Signals from each cell are processed and analysed using custom programs written in Matlab. Prior to each measurement the chip was flushed with 1M sodium hydroxide for 10 minutes to remove any residue followed by rinsing with deionised water. All buffers were filtered through a 0.22 μ m filter to avoid blockage by larger particles. The sample suspension was diluted to ensure that on average only one particle passed through the detection volume (360 μ m×40 μ m×28 μ m), with a typical cell concentration of around 500 cells/ μ L, mixed with beads at 200 beads/ μ L. Samples were measured at a flow rate of between 5 and 20 μ l/min, with a throughput of around 200 particles per second. Higher flow rates could be used but the signal quality is reduced due to quantization errors because of the limited sample rate on the impedance lock-in amplifiers.

Impedance chips

A photograph of the impedance chip $(20\mu m \times 15\mu m)$ is shown in Supplementary Figure 6. The chip is made from two glass wafers with nine Pt electrodes patterned on each side. One wafer is patterned with a thick resist to create a channel and the wafer pair bonded and diced to give individual chips. Fluid inlet and outlet holes are drilled using a laser. The measurement channel is $360\mu m$ long and $40~\mu m$ wide x $28\pm 2~\mu m$ high. All electrodes have a width of $30\mu m$ with a $10\mu m$ gap.

Cell culture

HL60 were cultured in RMPI 1640 + Glutamax with 10% Fetal Bovine Serum and 1% Penicillin-Streptomycin. Cell stock was kept in liquid nitrogen. Cells were thawed in a 37 °C water bath, washed and resuspended at a concentration of 5×10^5 cells/ml in fresh 20% FBS medium. Cell concentration was kept between 10^5 and 10^6 cells/ml and cells were maintained in 10% FBS medium. Cells were collected every two days after seeding when they were in the exponential growth phase (cell concentration never exceeded 1000 cells per μ l).

Methyl Cellulose (MC) buffer

Cells were resuspended in a buffer containing 0.5% w/v Methyl Cellulose (MC) in DPBS buffer made by dissolving dry MC powder (1 g in 200mL) as follows: To 70ml of DPBS heated to $80\,^{\circ}\text{C}$, add 1 g of MC powder and stir gently to disperse the powder. Add 130ml room temperature DPBS to the mixture with constant stirring to avoid clumping or aggregation (without heat). The MC mixture begins to hydrate as the temperature decreases and becomes jelly. After the solution has cooled to room temperature, place the mixture in the fridge for two hours to fully hydrate the MC. Buffers were stored in the refrigerator and prior to use were brought to room temperature and filtered through a $0.22\,\mu\text{m}$ filter.

Glutaraldehyde (GA)

For GA experiments, the cell concentrations were around 500 cells/ μ l. Cells were first suspended in PBS with different concentrations of Glutaraldehyde for 30 minutes at room temperature. After incubation, cells were centrifuged and resuspended in 0.5% MC in DPBS for deformability measurements. The same impedance chip was used for all GA experiments.

Osmotic shock

The osmolarity of the buffers was measured with a micro-osmometer (Loser). The osmolarity was increased by the addition of different amounts of D-mannitol to give 400, 500, 600 and 700 mOsm solutions. The conductivity of the solutions was measured using a conductivity meter. HL60 cells at a density of around 500 cells/µl were centrifuged at 180g for 5 min and then resuspended in the different buffers for 10 mins at 37°C (in an incubator). The same impedance chip was used for all osmotic shock experiments. Biological repeats were carried out with the same stock solutions to maintain an identical osmolarity for each group.

CytoD

Cells (1ml volume @ 500 cells/µl) were centrifuged and resuspended in 0.5% MC buffer. CytoD solutions were made by dissolving dry powder in dimethyl sulfoxide (DMSO) to give solutions of different molarity (2000, 200, 20, 2, 0.2 and 0.02µM) each with the same amount of DMSO (0.5% (v/v). Cells were mixed with 5µl of these stock solutions. Untreated cells (control) were also exposed to 0.5% v/v DMSO. Cells were exposed to CytoD at 37°C in an incubator for 10 minutes. CytoD is reversible therefore cells were not washed before measurement. Dose-response curves were obtained at flow rates of either 5 or 10 µl/min. Biological repeats were made on different days and within ten cell passages. The same impedance chip was used for all experiments, and the CytoD solutions were freshly prepared each time.

LatB

Stock solutions were made by dissolving 1mg of Latrunculin B dry powder in 1ml DMSO. Cells were centrifuged and resuspended in 0.5% MC buffer. LatB concentrations was 0.25μ M. Cells were exposed to LatB for 30 minutes, at 37°C in an incubator and were not washed prior to measurement. Biological repeats were conducted on different days and within ten cell passages.

Acknowledgements

The authors wish to acknowledge Katie Chamberlain for the manufacture of the microfluidic chips and Dr Emily Swindle for the gift of the HL60 cells.

Conflict of interest

The authors declare no conflict of interest.

References

- 1. Darling E.M and Di Carlo D. High-Throughput Assessment of Cellular Mechanical Properties. Annu Rev Biomed Eng. **17** 35-62. (2015).
- 2. Gupta V. and Chaudhuri O. Mechanical regulation of cell cycle progression and division Trends Cell Biol. **32** 773–785 (2022).
- 3. Gerum R., et al. Viscoelastic properties of suspended cells measured with shear flow deformation cytometry. eLife **11** e78823 (2022).
- 4. Suresh S. Biomechanics and Biophysics of Cancer Cells. Acta Biomaterialia. **3** 413–438 (2007).
- 5. Tse H T K, Gossett D.R., Moon Y.S., Masaeli M., Sohsman M., Ying Y., Mislick K., Adams R.P., Rao J. and Di Carlo D. Quantitative diagnosis of malignant pleural effusions by single-cell mechanophenotyping. Sci Transl. Med **5** 212ra163 (2013).
- Gossett D.R., Tse H.T.K., Lee S.A., Ying Y., Lindgren A.G., Yang O.O., Rao J., Clark A.T. and Di Carlo D., Hydrodynamic stretching of single cells for large population mechanical phenotyping PNAS 109 7630-7635 (2012).
- 7. Zak A., et al. Rapid viscoelastic changes are a hallmark of early leukocyte activation. Biophys J. **120** 1692-1704 (2021).
- 8. Bufi, N., Saitakis, M., Dogniaux, S., Buschinger, O., Bohineust, A., Richert, A., Maurin, M., Hivroz, C. and Asnacios, A. Human primary immune cells exhibit distinct mechanical properties that are modified by inflammation. Biophysical journal, **108** 2181-2190 (2015).
- 9. Sliogeryte K., Thorpe S.D., Lee D.A., Botto L and Knight M.K. Stem cell differentiation increases membrane-actin adhesion regulating cell blebability, migration and mechanics. Scientific Reports **4**, 7307 (2014).
- 10. Soteriou D., et al. Rapid single-cell physical phenotyping of mechanically dissociated tissue biopsies. Nature Biomedical Engineering **7** 1392–1403 (2023).
- 11. Hao Y., Cheng S., Tanaka Y., Hosokawa Y., Yalikun Y. and Li, M. Mechanical properties of single cells: Measurement methods and applications. Biotechnology Advances, **45** 107648 (2020).
- 12. Radmacher M. Studying the mechanics of cellular processes by atomic force microscopy. Methods Cell Biol. **83**, 347–372 (2007).
- Shan Y. and Wang H. The structure and function of cell membranes examined by atomic force microscopy and single-molecule force spectroscopy. Chem. Soc. Rev. 44 3617-3638 (2015).
- 14. Kang J.H., Miettinen T.P., Chen L., Olcum S., Katsikis G., Doyle P.S. and Manalis S.R. Non-invasive monitoring of single-cell mechanics by acoustic scattering Nature Methods **16** 263-269 (2019).
- 15. Guck J., Ananthakrishnan R., Mahmood H., Moon T.J., Cunningham C.C. and Kas J. The Optical Stretcher: A Novel Laser Tool to Micromanipulate Cells. Biophys. J. **81** 767-784 (2001).
- 16. Hochmuth, R. M. Micropipette aspiration of living cells. J. Biomech. 33 15–22 (2000).
- 17. Lange J.R. et al. Microconstriction arrays for high-throughput quantitative measurements of cell mechanical properties. Biophys. J. **109** 26–34 (2015).
- 18. Lange J.R., Metzner C., Richter S., Schneider W., Spermann M., Kolb T., Whyte G. and Fabry B. Unbiased high-precision cell mechanical measurements with microconstrictions. Biophys J **112** 1472-1480 (2017).
- 19. Nyberg K.D., Hu K.H., Kleinman S.H., Khismatullin D.B., Butte M.J., Rowat A.C. Quantitative deformability cytometry: rapid, calibrated measurements of cell mechanical properties. Biophys. J. **113**, 1574–1584 (2017).
- Byun S., Son S., Amodei D., Cermak N., Shaw J., Kang J.H., Hecht V.C., Winslow M.M., Jacks T., Mallick P. and Manalis S.R. Characterizing deformability and surface friction of cancer cells 110 7580-7585 (2013).

- 21. Chen J., Zheng Y., Tan Q., Shojaei-Baghini E., Zhang Y. L., Li J., Prasad P., You L., Wu X.Y. and Sun Y. Classification of cell types using a microfluidic device for mechanical and electrical measurement on single cells Lab Chip **11** 3174 (2011).
- 22. Adamo, A., Sharei A., Adamo L., Lee B., Mao S. and Jensen K.F. Microfluidics-based assessment of cell deformability. Analytical chemistry, **84**, 6438-6443. (2012).
- 23. Yang D., Zhou Y., Zhou Y., Han J. and Ai Y. Biophysical phenotyping of single cells using a differential multi-constriction microfluidic device with self-aligned 3D electrodes. Biosensors and Bioelectronics **133** 16–23 (2019).
- 24. Zhou Y., Yang D., Zhou Y., Khoo B. L., Han J. and Ai Y. Characterizing Deformability and Electrical Impedance of Cancer Cells in a Microfluidic Device. Anal. Chem. **90**, 912 (2018).
- 25. Kim J., Han S., Lei A., Miyano M., Bloom J., Srivastava V., Stampfe M.R., Gartner Z.J., LaBarge M.A. and Sohn L.L. Characterizing cellular mechanical phenotypes with mechano node-pore sensing. Microsystems & Nanoengineering **4** 17091 (2018).
- 26. Liu Y., Wang K., Sun X., Chen D., Wang J and Chen J. Advance of microfluidic constriction channel system of measuring single-cell cortical tension/specific capacitance of membrane and conductivity of cytoplasm. Cytometry **101** 434–447 (2022).
- 27. Otto E., et al. Real-time deformability cytometry: on-the-fly cell mechanical phenotyping. Nature methods, **12** 199-202 (2015).
- 28. Herbig F., M., Kräter, M., Plak, K., Müller, P., Guck, J. and Otto, O. Real-time deformability cytometry: label-free functional characterization of cells. Methods Mol Biol. **1678** 347-369 (2018).
- 29. Dudani J.S., Gossett D.R., Tse H.T.K. and Di Carlo D. Pinched-flow hydrodynamic stretching of single-cells. Lab Chip **13** 3728 (2013)
- 30. Guillou, L., Dahl, J.B., Lin, J.M.G., Barakat, A.I., Husson, J., Muller, S.J. and Kumar, S. Measuring cell viscoelastic properties using a microfluidic extensional flow device. Biophysical journal, **111** 2039-2050 (2016).
- 31. Armistead, F.J., De Pablo, J.G., Gadêlha, H., Peyman, S.A. and Evans, S.D. Cells under stress: an inertial-shear microfluidic determination of cell behavior. Biophysical Journal, **116** 1127-1135 (2019).
- 32. Urbanska M., Muñoz H.E., Shaw Bagnall J., Otto O., Manalis S.R., Di Carlo D. and Guck J. A comparison of microfluidic methods for high-throughput cell deformability measurements. Nature methods, **17** 587-593 (2020).
- 33. Honrado C., Michel N., Moore J.H., Salahi A., Porterfield V., McConnell M.J., and. Swami N.S. Label-Free Quantification of Cell Cycle Synchronicity of Human Neural Progenitor Cells Based on Electrophysiology Phenotypes ACS Sens. **6** 156–165 (2021b).
- 34. Jundi B., et al. Leukocyte function assessed via serial microlitre sampling of peripheral blood from sepsis patients correlates with disease severity. Nature biomedical engineering. **3** 961-973 (2019).
- 35. Jaffe A. and Voldman J. Multi-frequency dielectrophoretic characterization of single cells Microsystems & Nanoengineering **4** 23 (2018).
- 36. Gascoyne P. R. C. and Sangjo S. Isolation of Circulating Tumor Cells by Dielectrophoresis. Cancers (Basel). **6** 545–579 (2014).
- 37. McGrath J S., Honrado C, Moore J.H., Adair S J., Varhue W.B., Salahi A., Farmehini V., Goudreau B.J., Nagdas S., Blais E.M., Bauer T.W. and Swami N.S., Electrophysiology-based stratification of pancreatic tumorigenicity by label-free single-cell impedance cytometry. Anal Chim Acta **1101** 90-98 (2020).
- 38. Holmes D., Pettigrew D., Reccius C.H., Gwyer J.D., van Berkel C., Holloway J., Davies D.E., and Morgan H. Leukocyte analysis and differentiation using high speed microfluidic single cell impedance cytometry. Lab Chip **9** 2881-2889 (2009).

- 39. Honrado C., Ciuffreda L., Spencer D., Ranford-Cartwright L. and Morgan H. Dielectric characterization of Plasmodium falciparum-infected red blood cells using microfluidic impedance cytometry. J. R. Soc Interface. **15** 20180416 (2018).
- 40. Sun T and Morgan H. Single-cell microfluidic impedance cytometry: a review. Microfluid Nanofluid **8** 423–443 (2010).
- 41. Honrado C., Paolo Bisegna, Nathan S. Swami and Federica Caselli. Single-cell microfluidic impedance cytometry: from raw signals to cell phenotypes using data analytics. Lab Chip **21** 22-54 (2021a).
- 42. Spencer D and Morgan H. High-Speed Single-Cell Dielectric Spectroscopy ACS Sens. **5** 423–430 (2020).
- 43. Petchakup C., Yang, H., Gong, L., He, L., Tay, H.M., Dalan, R., Chung, A.J., Li, K.H.H. and Hou, H.W. Microfluidic impedance-deformability cytometry for label-free single neutrophil mechanophenotyping. Small, **18** 2104822 (2022).
- 44. Reale R, De Ninno A., Nepi T., Bisegna P and Caselli F. Extensional-Flow Impedance Cytometer for Contactless and Optics-Free Erythrocyte Deformability Analysis. IEEE Trans Biomed Eng. **70** 565-572 (2023).
- 45. Serhatlioglu M., Asghar M., Guler M.T. and Elbuken C. Impedance-based viscoelastic flow cytometry Electrophoresis **40** 906-913 (2019).
- 46. Spencer D and Morgan H. Positional dependence of particles in microfluidic impedance cytometry Lab Chip, **11** 1234 (2011).
- 47. De Ninno A., Errico V., Bertani F.R., Businaro L., Bisegna P and Caselli F. Coplanar electrode microfluidic chip enabling accurate sheathless impedance cytometry Lab on a Chip **17** 1158-1166 (2017).
- 48. Daguerre H., Solsona M., Cottet J., Gauthier M., Renaud P and Bolopion A. Positional dependence of particles and cells in microfluidic electrical impedance flow cytometry: origin, challenges and opportunities. Lab Chip **20** 3665 (2020).
- 49. Reale R., De Ninno A, Businaro L., Bisegna P and Caselli F. High-throughput electrical position detection of single flowing particles/cells with non-spherical shape. Lab on a Chip **19** 1818-1827 (2019).
- 50. Guo, M., Pegoraro, A.F., Mao, A., Zhou, E.H., Arany, P.R., Han, Y., Burnette, D.T., Jensen, M.H., Kasza, K.E., Moore, J.R. and Mackintosh, F.C. Cell volume change through water efflux impacts cell stiffness and stem cell fate. Proceedings of the National Academy of Sciences, 114 E8618-E8627 (2017).
- 51. Sukhorukov V.L., Arnold W.M. and Zimmermann U. Hypotonically Induced Changes in the Plasma Membrane of Cultured Mammalian Cells. J. Membrane Biol. **132** 27-40 (1993).
- 52. Pietuch A., Brückner B.R. and Janshoff A. Membrane tension homeostasis of epithelial cells through surface area regulation in response to osmotic stress. Biochim. Biophys. Acta **1833** 712-722 (2013)
- 53. Guzniczak, E., Otto, O., Whyte, G., Willoughby, N., Jimenez, M. and Bridle, H. Deformability-induced lift force in spiral microchannels for cell separation. Lab on a Chip, **20** 614-625 (2020).
- 54. Forsyth A.M., Wan J., Ristenpart W.D. and Stone H.A. The dynamic behavior of chemically "stiffened" red blood cells in microchannel flows. Microvascular Research **80** 37–43 (2010).
- 55. Cheung, K., Gawad S., and Renaud P. Impedance spectroscopy flow cytometry: on-chip label-free cell differentiation. Cytometry Part A **65** 124-132 (2005).
- 56. Gagnon Z., Gordon J., Sengupta S. and Chang H-C. Bovine red blood cell starvation age discrimination through a glutaraldehyde-amplified dielectrophoretic approach with buffer selection and membrane cross-linking. Electrophoresis **29** 2272–2279 (2008).
- 57. Pribush A., Meyerstein D. and Meyerstein N. Kinetics of erythrocyte swelling and membrane hole formation in hypotonic media. Biochim Biophys Acta Biomembr. **1558** 119-132 (2002).

58. Golfier, S., Rosendahl, P., Mietke, A., Herbig, M., Guck, J. and Otto, O. High-throughput cell mechanical phenotyping for label-free titration assays of cytoskeletal modifications. Cytoskeleton, **74** 283-296 (2017).